frontiers | Frontiers in Physics

TYPE Review
PUBLISHED 06 December 2022
DOI 10.3389/fphy.2022.1058419

OPEN ACCESS

EDITED BY
Leandro Gasques,
University of São Paulo, Brazil

REVIEWED BY
Marco La Commara,
University Federico II, Italy
Georgios Souliotis,
National and Kapodistrian University of Athens, Greece

*CORRESPONDENCE
N. S. Martorana,
martorana@lns.infn.it

SPECIALTY SECTION
This article was submitted to Nuclear Physics,
a section of the journal
Frontiers in Physics

RECEIVED 30 September 2022
ACCEPTED 03 November 2022
PUBLISHED 06 December 2022

CITATION
Martorana NS, Cardella G, Guazzoni C, Pagano EV, Russo AD, Russotto P, Acosta L, Amato A, Calabretta L, Caruso A, Cavallaro S, Cosentino L, Costa M, De Filippo E, De Luca G, Geraci E, Gnoffo B, Maiolino C, Passarello S, Pirrone S, Politi G, Pulvirenti S, Risitano F, Rizzo F, Santonocito D, Trifiró A, Trimarchi M, Tudisco S and Vecchio G (2022), Radioactive ion beam opportunities at the new FRAISE facility of INFN-LNS. *Front. Phys.* 10:1058419. doi: 10.3389/fphy.2022.1058419

Radioactive ion beam opportunities at the new FRAISE facility of INFN-LNS

N. S. Martorana[1,2]*, G. Cardella[3], C. Guazzoni[4], E. V. Pagano[2], A. D. Russo[2], P. Russotto[2], L. Acosta[4,5], A. Amato[2], L. Calabretta[2], A. Caruso[2], S. Cavallaro[2], L. Cosentino[2], M. Costa[2], E. De Filippo[3], G. De Luca[2], E. Geraci[1,3], B. Gnoffo[1,3], C. Maiolino[2], S. Passarello[2], S. Pirrone[3], G. Politi[1,3], S. Pulvirenti[2], F. Risitano[3,6], F. Rizzo[1,2], D. Santonocito[2], A. Trifiró[3,6], M. Trimarchi[3,6], S. Tudisco[2] and G. Vecchio[2]

[1]Dipartimento di Fisica e Astronomia "Ettore Majorana", Universitá Degli Studi di Catania, Catania, Italy, [2]INFN-LNS, Catania, Italy, [3]INFN-Sezione di Catania, Catania, Italy, [4]DEIB Politecnico Milano and INFN Sez, Milano, Italy, [5]Instituto de Física, Universidad Nacional Autónoma de México, Mexico City, Mexico, [6]Dipartimento MIFT, Universitá di Messina, Messina, Italy

At the Laboratori Nazionali del Sud of INFN (INFN-LNS) in Catania, the construction of the new Radioactive Ion Beams (RIBs) facility FRAISE (FRAgment In-flight SEparator) has reached its ending phase. The facility uses the in-flight technique based on a primary beam fragmentation impinging on light Be or C targets. FRAISE makes use of light and medium mass primary beams, having power up to ≈ 2–3 kW, leading to RIBs, whose intensities vary in the range of ≈ 10^3–10^7 pps, for nuclei far from and close to the stability valley, respectively. FRAISE aims at providing high-intensity and high-quality RIBs for nuclear physics experiments, also serving to interdisciplinary research areas, such as medical physics. Critical aspects for high-quality beams are the tuning and transport, representing time-consuming processes and requiring dedicated diagnostics and tagging devices measuring many features of RIBs. Some of these devices should be capable to operate in radioactively activated environments because of the expected 2 kW beam lost in the dipole after the production target. Due to its peculiar robustness to radioactive damage, Silicon Carbide (SiC) technology has been considered for the detection layer. In this view, an R&D campaign has been started aiming at developing the FRAISE facility, the new diagnostics system, and a new tagging device, the latter of which will be useful for the CHIMERA multidetector beamline. In this paper, we discuss the status and the perspectives of the facility with a focus on the RIBs opportunities.

KEYWORDS

RIBs, FRAISE, unstable nuclei, in-flight technique, SiC

Introduction

Physics with high-intensity RIBs ($\geq 10^6$ pps), especially in the case of nuclei far from the beta stability valley, is one of the most attractive directions of modern nuclear physics. The attempt of observing peculiar properties of unstable nuclei, not observed in the stable ones, is the compass of such strong interest. Most of the current knowledge on the nuclear structure is limited to nuclei close to the stability valley, and only surveys made possible by the availability of RIBs allow for further exploring such knowledge in uncharted territories of the nuclei chart [1–6]. The presence of molecular structures of α clusters, which might lead to special excited states, such as rotational bands, is among the phenomena to be possibly investigated in unstable nuclei [7, 8]. The impact of studying clustering structures made of α particles in neutron-rich isotopes of Be, B, and C, with molecular-like behavior, is quite relevant for advancing knowledge on the nuclear strong interaction [7–9]. Other unstable nuclei properties can be probed. Among these, the neutron excess in light neutron-rich nuclei turns into the creation of nuclear halos, whose structures are not all the same, such as the di-neutron one, in which the halo is made of two neutrons [10, 11]. In the same context, for heavier nuclei, the neutron excess forms a neutron skin, which can lead to particular excitation modes [12]. Neutron halos and skins can contribute in altering the radius and the density of nuclei, also affecting the established sequence of magic numbers of the shell model, and, hence, further imply potential improvement of the nuclear models. Moreover, halos/skins have relevant connections with the Equation of State of nuclear matter (EoS), and understanding more about these properties would allow one to provide stronger constraints to the knowledge of the EoS. Beyond the neutron halo, several works also suggest the existence of a proton-halo [11, 13–17].

RIBs research becomes relevant also in the astrophysical context, where reactions involving unstable nuclei occur in some nucleosynthesis processes, such as the *r*-process, beyond the stellar nucleosynthesis. Despite most of the energy production in stars occurs by nuclear reactions between stable nuclei, in fact violent reactions in supernovae explosions or astrophysical events at high temperature and/or densities, often involve nuclear reactions with radionuclides [18, 19]. The study of the cross sections of these reactions could provide more information about the aforementioned processes.

New research perspectives face to the nuclear isospin physics. By using RIBs it is possible to extend these studies to heavy-ion reactions at Fermi energies with high isospin asymmetries, with important consequences also in the EoS research field. Finally, unstable nuclei can be largely used for the production of radiopharmaceuticals and for pioneeristic medical physics applications [20–22].

RIBs, therefore, provide a unique tool for studying the properties of nuclei and nuclear matter away from normal conditions found in stable nuclei. The most important base of these research works is the production of RIBs with high-intensity and good quality. Radioactive nuclei are experimentally accessible, thanks to the development of production techniques based on two methods: the In-Flight fragmentation method and the Isotope Separation On Line (ISOL) technique [23]. The advantage of the ISOL method is the quality of the beam, in terms of energy resolution and low emittance. On the other hand, the ISOL method is not advised for producing short-lived nuclei. The In-Flight fragmentation method is based on the fragmentation of a stable beam, typically a heavy-ion beam, on a thin target. The unstable beams are formed with a forward focusing and are subsequently selected and transported with the use of a fragment separator, mainly based on magnetic elements. This method is the one suited to produce short-lived isotopes [24]. For all the aforementioned reasons, radioactive nuclei production facilities have been developed worldwide, and upgrades and new constructions are underway to produce high-intensity RIBs [20, 25–29].

In the following sections, the new progress obtained at INFN-LNS for the production of RIBs is reported, with a focus on the RIBs opportunities and also on physics cases of interest.

The FRAISE facility at INFN-LNS

The INFN-LNS scientific community is involved in an upgrade project, named POTLNS, of accelerating infrastructures designed for the research in nuclear physics [30]. The upgrade provides a new extraction system of the superconducting cyclotron (CS) based on the stripping method, stepping beyond the electrostatic deflection system, for reaching a larger CS power. The stripping method will be very efficient for ion beams in the Fermi energy range and with mass numbers A up to ≈40 [31–34]. To exploit the high beam power provided by the improved CS, the POTLNS project has included the construction of a new in-flight apparatus for high-intensity radioactive ion beams production, named FRAISE (FRAgment In-flight SEparator) [31–34]. A long-standing expertise was indeed gained at INFN-LNS in this field, thanks to the FRIBs (in Flight Radioactive Ion Beams) apparatus [35, 36], operating since 2001 using a primary beam power lower than ≈100 W. The FRIBs facility used a beryllium target, placed after the first dipole of the CS extraction line, to induce the fragmentation of the primary beam. The beam resulting from the in-flight method contains several stable and unstable ions. The use of magnetic fields, which make the so-called fragment separator (FRS), is then necessary to select and to transport the ions of interest for a specific study. The FRS, indeed, permits to maximize the yield of the ions of interest, reducing the presence of unwanted beams. In FRIBs, the selection was performed by a fragment separator made of two 45° bending angle dipoles. Figure 1 (left side) displays a map of INFN-LNS before the

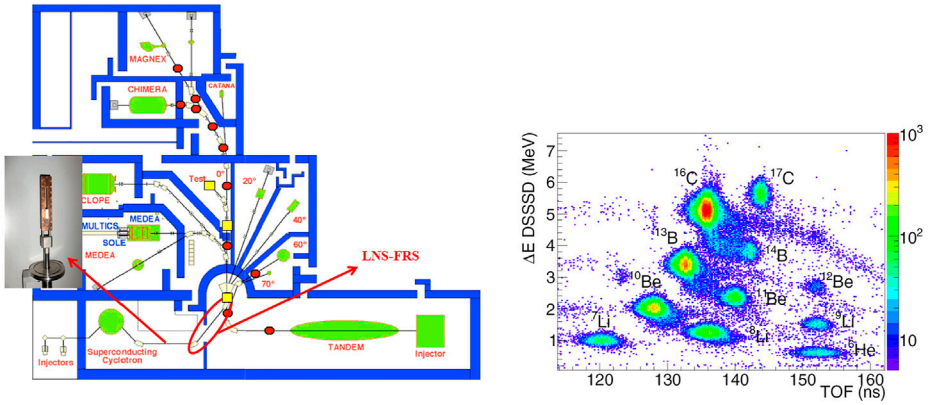

FIGURE 1
Left: map of the INFN-LNS before the upgrading project. The fragment separator is located inside the red ellipse. The photo in the inset shows the beryllium target system. Dots indicate diagnostics elements made of plastic scintillators, while squares indicate diagnostics elements based on double-sided silicon strip detectors, figure adapted from [33]. Right: ΔE-TOF correlation plot obtained with the tagging system used in the CHIMERA beamline, for a cocktail beam produced by ^{18}O beam of 55 AMeV on a 1500 μm thick ^{9}Be target, figure adapted from [9].

upgrading project, also showing the position of the FRS and a picture of the beryllium target system. The magnetic selection by the use of the fragment separator could not separate ions with the same A/Q ratio, where A indicates the mass number and Q indicates the charge that in case of light nuclei is equal to the Z atomic number, and inside the magnetic elements acceptance of the $\Delta p/p \approx 1.2\%$. The final result was a cocktail beam composed of several ions, in which the yield of the beam of interest was maximized. Because of this, an event-by-event characterization of beam components arriving on the target point was essential in order to off-line select the ion of interest. As an example, in the CHIMERA beamline such characterization was performed using a tagging device and ΔE-TOF technique [37]. The tagging device was composed by using a micro channel plate detector, which produced the start signal for the TOF measurement, and a double-sided silicon strip detector (DSSSD) (140–150 μm thick) downstream, which provided the stop signal for the TOF measurement, the energy loss (ΔE) signal and information on the beam profile. A parallel plate avalanche counter (PPAC) detector was also used for reconstructing some information on the beam trajectory. Figure 1 (right side) shows an example of the ΔE-TOF correlation plot, as given by the tagging system of the CHIMERA beamline [31], for a ^{18}O primary beam at 55 AMeV impinging on a 1500 μm thick ^{9}Be target and a magnetic rigidity selection of $B\rho \approx 2.8$ Tm [9]. Furthermore, in the FRIBs apparatus, several diagnostics elements were used along the beamline. The purpose of such diagnostics elements was the achievement of an optimal transport, from the beryllium production target to the point of end use. The diagnostics elements were made of plastic scintillators, which allowed for a measurement of the beam total yield, and of DSSSDs segmented in 16 × 16 strips, each of them with an active area of 3 × 48 mm^2 that permitted a beam profile reconstruction with a pixel resolution of 3 × 3 mm^2. The use of plastic scintillators was particularly useful in the RIBs case, where low-intensities did not allow the use of standard methods, such as the use of alumina coupled to optical cameras. In addition, by the ΔE-TOF method, where the start was provided by the CS radiofrequency signal while the stop signal and the ΔE energy loss were provided by the DSSSDs, it was possible to carry out an event-by-event identification of the fragmentation beam along the beamline [33, 37]. Figure 1 (left side) also displays the location of plastic scintillators (dots) and DSSSDs (squares). In some cases, the use of a wedge/degrader, inserted between the two 45° dipoles, allowed the differentiation, in magnetic rigidity, of the different species of the cocktail beam having the same A/Q ratio, performing a more efficient rejection of unwanted ions and permitting to obtain a cocktail beam with a high purity of a specific ion. As an example, this method was used during the OTPC@LNS experiment, where a ^{11}Be beam with purity of ≈95% was produced, to study the β-delayed α emission from ^{11}Be with an optical time projection chamber, see Ref. [33] and references therein for details. Thanks to the FRIBs facility, several RIBs from ^{6}He to ^{68}Ni at Fermi energies were successfully exploited in experiments [9, 38–40].

The limitation of FRIBs was due to the maximum power delivered by the CS (100 W). For this reason, research has focused on nuclei near the stability valley, being yields for nuclei far from stability insufficient to perform experiments with enough statistics.

Due to the impossibility of installing a shielding infrastructure in the FRIBs location, the best solution for exploiting the possibilities provided by the CS upgrading has been the building of the new fragment separator FRAISE.

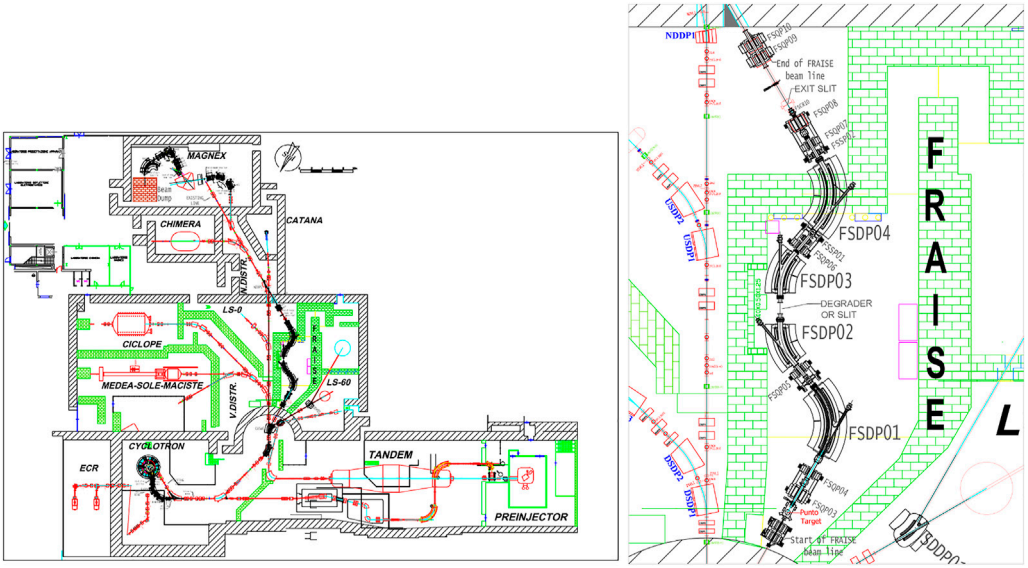

FIGURE 2
Left: view of the INFN-LNS beamlines and halls, in which the position of the FRAISE apparatus is evident. Right: scheme of the FRAISE facility [32].

FRAISE is hosted in a shielded area (bunker) of the INFN-LNS, previously hosting the LS-20 and LS-40 experimental halls, as schematically shown in Figure 2 (left side). The bunker in that area allows delivering primary beams of power up to ≈ 2–3 kW. Within this primary beam power, FRAISE allows the production of RIBs with intensity from 10^3 pps to 10^7 pps, for nuclei far and close from the stability, respectively. Such intensities increase the yield by a factor of ≈20 with respect to the FRIBs facility [31, 33]. The improvement in intensity reachable with FRAISE opens the way to more precise studies on nuclei close to the stability line and to extend investigations to nuclei far from the stability, contributing significantly to the overall picture of nuclear physics with unstable beams. The region that will host FRAISE will be managed to allow a safe air treatment and an appropriate shielding of walls, floor, and roof. The latter ones will be made with materials suitable for slowing down and absorbing radiations, especially produced by neutrons and γ, and to avoid contamination in adjacent halls. Furthermore, a dedicated radio protection system for the first magnetic dipole will be required. This dipole represents a crucial point because the residual primary beam, stopped in the dipole, deposits a high dose there [31, 33].

The new production target, CLIM [41], is housed in a dedicated chamber. It consists of a beryllium- or carbon-rotating disk, of appropriate thickness, allowing distribution of the primary beam impact area on a circular crown of ≈10–15 cm mean radius, maintaining the degradation and heating of the target under control. The target will be significantly activated, after and during experiments, and it will be impossible to remove it manually. Because of this, a dedicated system for automatic change and remote handling of targets has been designed and will be built soon. The fragment separator consists of two symmetric branches, to ensure optimal achromatic conditions and reduce magnetic field high order effects, due to the large acceptance typical of a separator device. The extraction line upstream target chamber has been designed with a condition of energy achromatism to deliver a much focused spot size of stable beam at the target position, in order to optimize the outgoing cocktail beam [32]. In detail, the FRAISE line is made of four dipoles, six quadrupoles, and two sextupoles, as shown in Figure 2 (right side). The list of magnetic devices and their features are reported in Table 1.

Two chambers will also be installed in the beamline to house slits and diagnostics systems. The first chamber located in correspondence with the plane of symmetry between the two branches, the greatest energy dispersion point, and the second one located at the exit of the fragment separator. The slit on the symmetry plane can be used to vary the acceptance $\Delta p/p$ of the fragment separator, in order to reduce the energy dispersion of the outgoing components, while the exit slit can be used to reduce and, eventually, remove unwanted ions in the cocktail beam. An aluminum degrader/wedge can be introduced after the central slit, in order to perform a better rejection of contaminants, following the method used in the FRIBs facility. However, the use of a wedge/degrader can worsen the final quality of the beam, although improving its purity. The FRAISE line has been designed to get a maximum magnetic rigidity equal to 3.2 Tm, a momentum acceptance of 1.2%, and a solid angle acceptance of ≈2.5 msterad. The FRAISE line has ≈5 m of momentum dispersion at the symmetry plane, and this means an energy

TABLE 1 FRAISE magnetic transport element features [32].

Element	Name	Quantity	Feature
Dipole	FSDP01 and FSDP04	2	R = 2 m α = 70° and B = 0.66–1.65 T
Dipole	FSDP02 and FSDP03	2	R = 2 m α = 40° and B = 0.66–1.65 T
Quadrupole	FSQP03 and FSQP08	2	ϕ = 104 mm and Gmax = 14.1 T/m
Quadrupole	FSQP04 and FSQP07	4	ϕ = 132 mm and Gmax = 5.77 T/m
Sexstupole	FSSP01 and FSSP02	2	ϕ = 130 mm and Gmax = 59.2 T/m^2

resolving power of 2600 with a beam spot size of 1 mm [32]. Thanks to the high energy dispersion value at the symmetry plane, FRAISE also allows the reduction of the energy spread of the primary beam. For example, it will be possible to obtain an energy spread of 0.1%, as mandatory for the NUMEN experimental program [42]. It says that FRAISE can also be used as precise energy selector, for those experiments requiring stable beams with very small energy dispersion.

Diagnostics and tagging systems

Critical aspects for high-quality beams are the tuning and transport, representing time-consuming processes and requiring dedicated diagnostics and tagging devices measuring different RIBs features. The same devices should be capable to operate in radioactively activated environments because of the expected high direct and background irradiation and to sustain several experiments per year. For the diagnostics detection layers due to its robustness to radioactive hardness, SiC technology has been considered [43]. Such choice is also confirmed by feasibility studies carried out by simulations and preliminary tests [33, 44]. The diagnostics system will be versatile to allow its use as a beam monitor, tagging element, and eventually active wedge, providing information about isotopic identification, intensity, energy, position, and to some extent trajectory of the beams. The RIBs composition will be determined by measuring the ΔE energy loss of ions and the TOF between two detection systems, or with respect to a reference time signal synchronous with the primary beam arrival on the production target, as the cyclotron radiofrequency signal. In detail, the system consists of two arrays, each one made of single detection pads with an active area of 5 mm × 5 mm monolithically assembled in 2 × 2 and a thickness of 100 μm. By composing an array of several pads in rows and columns, it is possible to cover an area of the order of ≈60 mm × 30 mm, wide enough for typical RIB profiles in the high dispersion point. Such segmentation sustains a maximum value of ≈ 10^7 pps over the whole array. A sandwich configuration of two detection arrays located at a distance of few cm and with a half-pitch shift both in X and Y, and readout in coincidence improves the position resolution and partially recover for the dead region around each sensor die, thus allowing to reach efficiencies larger than 90%. Figure 3 shows a scheme of the SiC arrays. The same device could be used not only as a diagnostics element but also as a tagging one for the CHIMERA multidetector beamline. In this case, it will be necessary to have an event-by-event tagging of the cocktail beam, using the ΔE-TOF method and the trajectory measurement.

For the final configuration, the detector active area will be logically divided into four segments, each bonded to a different carrier area and connected to a dedicated custom frontend card, as schematically shown in Figure 4A.

Particular care has been taken to minimize the material budget along the beam path. To this aim, we developed a custom layer stacking for the carrier, which is able to reduce the material thickness in the detector area to 300 μm while leaving the conventional thickness and rigidity in the outer area used for interconnections and for handling. Figure 4B shows the cross section of the chosen layer stacking, and Figure 4C shows the photograph of the mini-carrier developed for a 1 cm^2 active area detector prototype or for four 5 mm × 5 mm that can be glued with minimized gap in a window-like configuration. The reduced thickness area is evident as transparent to light. The objective is, however, to reduce this thickness to zero for the final design. We carried out a preliminary qualification of the detector properties on the first 5 mm × 5 mm detector prototypes, and the CV measurements show the expected 21 pF detector capacitance at about 400 V depletion voltage. The final system will be housed in a DN160 spherical cross to be located along the beam path and to be easily interchangeable as it is in a high dose region and is activated when removed. Figure 5 shows a sketch of the cross section of the proposed arrangement. A lateral movable arm holds the detection system, so that it can be removed or inserted along the beam path, according to experimental needs. We designed a dedicated frontend in charge preamplifier configuration with fast decay to readout the full detection system [45, 46]. The first 4-channel boards have been produced and qualified. As a compromise among performance, cost, and versatility, we probed the use of conventional high-performance operational amplifiers for the forward gain stage [47]. Figure 6 shows the measured output waveforms of the first designed 4-channel prototype, for different

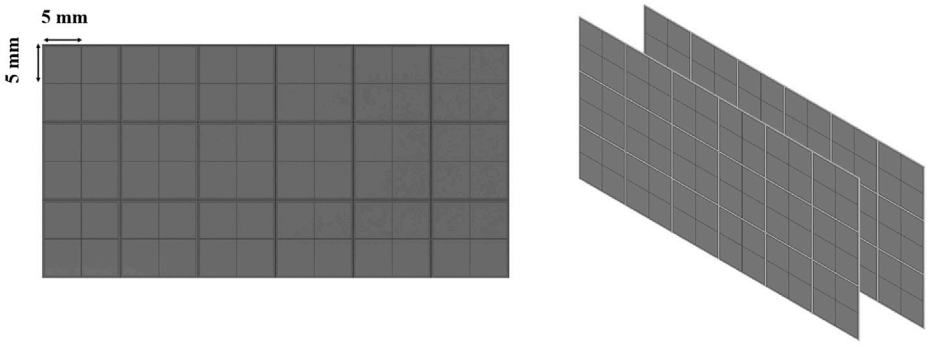

FIGURE 3
Scheme of the SiC detection system for the diagnostics and tagging devices of the FRAISE facility: frontal (left) and side (right) views.

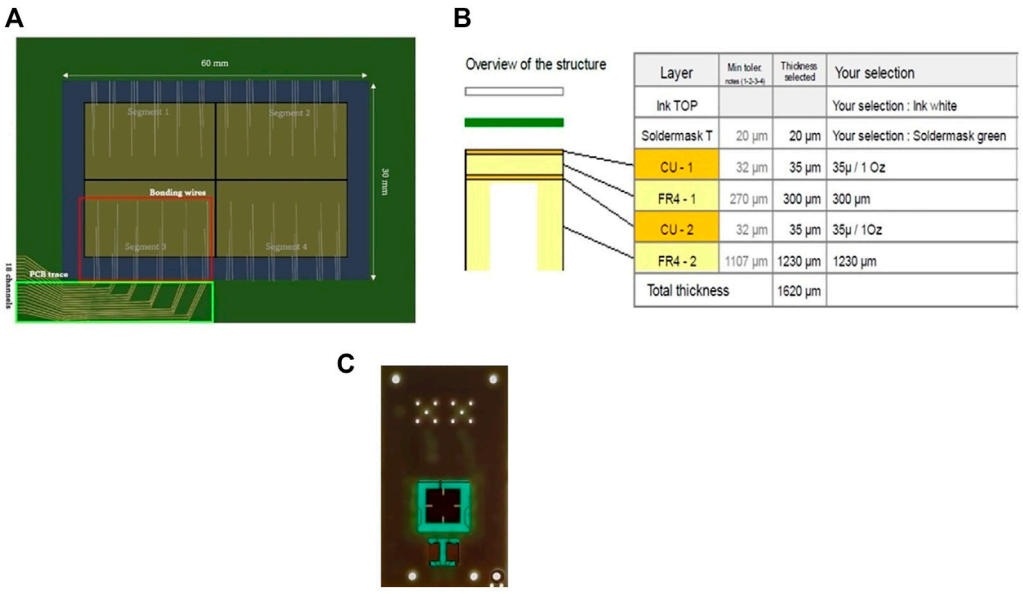

Layer	Min toler.	Thickness selected	Your selection
Ink TOP			Your selection : Ink white
Soldermask T	20 µm	20 µm	Your selection : Soldermask green
CU - 1	32 µm	35 µm	35µ / 1 Oz
FR4 - 1	270 µm	300 µm	300 µm
CU - 2	32 µm	35 µm	35µ / 1Oz
FR4 - 2	1107 µm	1230 µm	1230 µm
Total thickness		1620 µm	

FIGURE 4
(A) Preliminary bonding scheme of the full detection layer, covering an active area of 30 mm × 60 mm. **(B)** Cross section of the chosen layer stacking for the detector holder that minimizes the material budget along the beam path. **(C)** Photograph of the mini-carrier developed for a 1 cm^2 active area detector prototype. The reduced thickness area is evident as transparent to light.

amplitudes of the injected test signal, indicated as SiC deposited energy.

LISE++ simulations

Simulations using the LISE++ tool unveiled the FRAISE possibilities for the production of RIBs [34]. In these simulations, we included an aluminum 100 μm thick homogenous degrader placed on the symmetry plane and a 100 μm thick SiC detector placed at the exit of the fragment separator, used as a tagging detector. The results have been obtained using primary beams, whose extraction by stripping in the upgraded CS has been studied in detail and assuming 2 kW of power for the primary beam [48]. These primary beams are listed in Table 2, together with the energy and the beam power used as input for simulations [34]. It has to be noted that these primary beams can also be accelerated at lower energies.

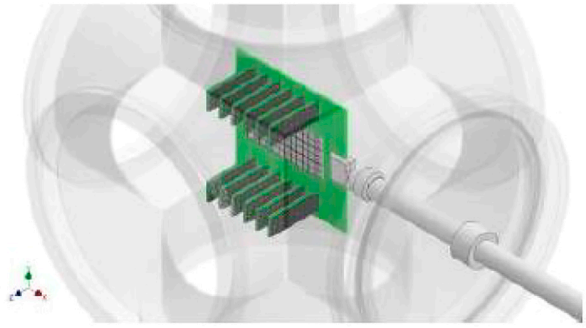

FIGURE 5
Sketch of the proposed detection system in its final configuration. The system is housed in a DN160 spherical cross element along the beam path and can be moved out of the beam *via* a lateral arm.

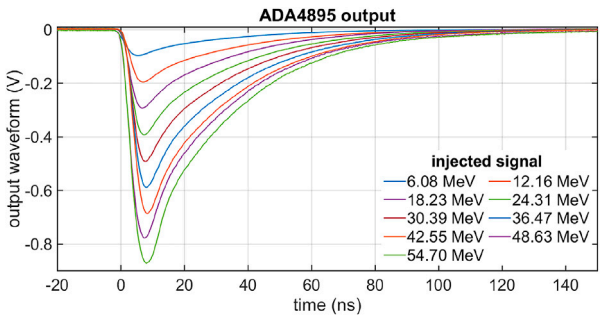

FIGURE 6
Output waveforms of the first designed 4-channel prototype, for different amplitudes of the electrical test signal.

TABLE 2 Primary beams, whose extraction by stripping has been studied in detail, with relative energy and power used as input for the simulations.

Ion	Energy (AMeV)	Power (kW)
$^{12}C^{6+}$	60	2
$^{18}O^{8+}$	70	2
$^{20}Ne^{10+}$	70	2
$^{40}Ar^{18+}$	60	2

However, the primary beam energy has to be ≈25 AMeV in order to make the projectile fragmentation reaction possible, producing RIBs of appreciable intensities. As additional information, the use of primary beams of lower energies will cause a decrease of ≈1 order of magnitude for the expected intensities and final energies of 20–25 AMeV. For each isotope of interest, we used a ^{9}Be production target with optimized thickness, and the fragment separator has been set to allow a clear separation of the isotope of interest from contaminants in the simulated ΔE-TOF tagging plot. The ΔE was given by the simulated value of the energy deposited in the SiC detector, while the TOF was given by the simulated time difference between the start provided by the radiofrequency signal of the CS, and the stop given by the SiC detector.

Figure 7 reports the expected intensities and the average energies at the exit of the fragment separator for RIBs produced using primary beams $^{12}C^{6+}$ at 60 AMeV (left side) and $^{18}O^{8+}$ at 70 AMeV (right side). The expected intensities are of ≈10^{7}–10^{8} pps for RIBs near the stability valley, and ≈10^{3}–10^{4} pps for nuclei far from the stability valley. As an example, Figure 8 shows the expected spatial distribution at the exit of the fragment separator on the horizontal direction (left) and the simulated ΔE-TOF tagging plot (right) in the case of $^{18}O^{8+}$ at 70 AMeV primary beam, and tuning of the fragment separator maximizing the ^{13}B production, being 65% of the whole cocktail beam produced. Figure 9 (top) shows the same information as in Figure 7 but in the case of a primary beam of $^{20}Ne^{10+}$ at 70 AMeV. It can be observed that these light primary beams will efficiently span a relevant part of both neutron poor and rich unstable nuclei with A ≤ 20. Figure 9 (bottom) shows the results for a primary beam of $^{40}Ar^{18+}$ at 60 AMeV, highlighting the wide possibilities of an efficient production of unstable isotopes of K, Ar, Cl, S, P, Si, and Al.

The use of other primary beams needs studies concerning the feasibility of extraction through the stripping channel, i.e., detailed studies of acceleration trajectories inside the CS and of the achievable output power, depending also on the maximum injection currents given by the available ion sources. However, other beams, in addition to the aforementioned ones, will allow to further extend the already rich offer. As in the case of relevant interest, we can mention the ^{13}C beam, which is relevant to increase the yield of neutron-rich B, Be, and Li isotopes; the ^{16}O beam, allowing to increase, with respect to what already is shown, the yield of neutron poor oxygen isotopes; the ^{22}Ne beam allowing to increase the yield of neutron-rich F, O, and N isotopes; and the ^{36}Ar beam for a better production of neutron poor isotopes, as shown in Figure 9 (bottom). These primary beams are very similar to the ones here presented in detail, whose feasibility should not present huge difficulties. In addition, primary beams of ^{24}Mg, ^{27}Al, and ^{32}S could be used for producing RIBs in the region of mass number between 20 and 31, where isotopes of S, P, Si, Al, Mg, and Na lie. The use of heavier primary beams, such as ^{54}Ni, ^{48}Ca, or ^{70}Zn, could also be relevant for the production of isotopes in the region of A ≥40 [49], and it will be studied in the near future, after the CS characterization that takes place during the commissioning phase. As an example, using a ^{70}Zn primary beam at 40 AMeV will be possible to produce ^{68}Ni with 8.5 × 10^{5} pps and 70% of purity. Figure 10 shows the expected spatial distribution at the exit of the fragment separator on the horizontal direction (left) and the simulated ΔE-TOF tagging

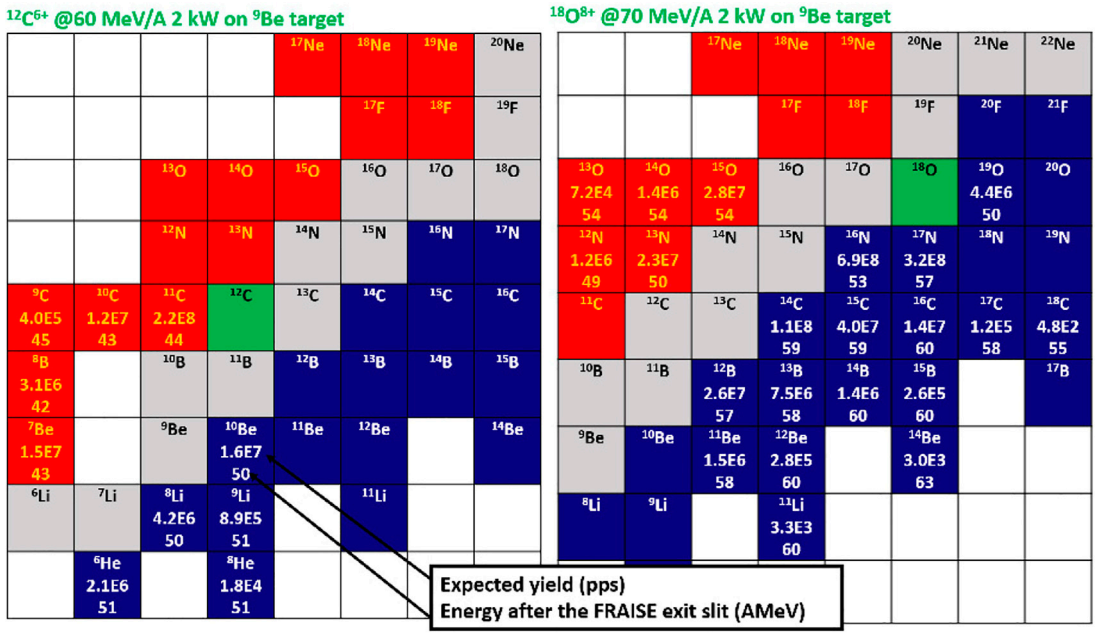

FIGURE 7
Left: simulation of RIBs that can be produced with FRAISE, using ^{12}C as the primary beam. Right: same as left, using ^{18}O as primary beam. The figure is taken from [34].

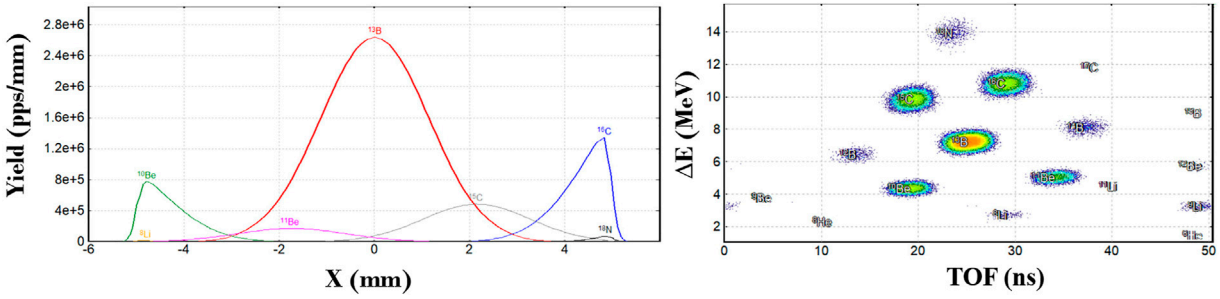

FIGURE 8
Simulated spatial distribution at the exit of the fragment separator on the horizontal direction (left) and simulated ΔE-TOF tagging plot (right), in the case of $^{18}O^{8+}$ at 70 AMeV primary beam and for a tuning of the fragment separator maximizing the ^{13}B production. For the sake of clarity, only the main contaminants are shown in the spatial distribution plot.

plot (right). In this case, we used, as input for the simulation, a beam power of 1 kW. For heavy primary beams, as ^{70}Zn, some issues due to the presence of charge states have to be taken into account. Indeed, with the new extraction system, based on the stripping method, in the case of heavier ions different charge states will be produced. While the chosen charge state goes into the extraction channel, the other ones dissipate their energy inside the CS. This could allow for an excessive heating of the CS. To overcome this problem, it is necessary to limit the intensity of the primary beam. Moreover, using the ^{48}Ca primary beam at 50 AMeV is possible to produce ^{46}Ar with 4.16×10^6 pps and 80% of purity. Figure 11 shows the expected spatial distribution at the exit of the fragment separator on the horizontal direction (left) and the simulated ΔE-TOF tagging plot (right).

Furthermore, we also performed simulations, using ^{27}Al and ^{50}Ti targets, in order to investigate the neutron pickup possibility that is offered in the reactions at the Fermi energies [50–52], allowing to enhance the neutron-rich nuclei yield. However, we

$^{20}Ne^{10+}$ @70 MeV/A 2 kW on ^{9}Be target

^{17}Ne 8.7E5 53	^{18}Ne 3.1E7 51	^{19}Ne 6.0E8 52	^{20}Ne	^{21}Ne	^{22}Ne	^{23}Ne	^{24}Ne
	^{17}F 1.7E8 50	^{18}F	^{19}F	^{20}F 9.5E6 55	^{21}F	^{22}F	^{23}F
^{15}O	^{16}O	^{17}O	^{18}O	^{19}O	^{20}O	^{21}O	^{22}O
^{14}N	^{15}N	^{16}N	^{17}N	^{18}N 3.7E6 57	^{19}N	^{20}N	^{21}N
^{13}C	^{14}C	^{15}C	^{16}C	^{17}C	^{18}C	^{19}C	^{20}C
^{12}B	^{13}B	^{14}B	^{15}B		^{17}B		^{19}B
^{11}Be	^{12}Be		^{14}Be				
	^{11}Li						

$^{40}Ar^{18+}$ @60 MeV/A 2 kW on ^{9}Be target

				^{35}K	^{36}K 6.6E3 48	^{37}K 8.2E4 48	^{38}K 6.3E5 49	^{39}K	^{40}K	^{41}K	^{42}K 1.3E6 41	^{43}K 2.6E3 40
	^{31}Ar	^{32}Ar	^{33}Ar	^{34}Ar	^{35}Ar 8.9E5 45	^{36}Ar	^{37}Ar 9.2E7 42	^{38}Ar	^{39}Ar 1.3E9 43	^{40}Ar	^{41}Ar 1.0E7 47	^{42}Ar 2.2e4 42
		^{31}Cl	^{32}Cl 4.6E4 46	^{33}Cl 1.2E6 46	^{34}Cl 1.5E7 42	^{35}Cl	^{36}Cl	^{37}Cl	^{38}Cl 7.4E8 39	^{39}Cl 3.2E8 44	^{40}Cl 4.9E6 44	^{41}Cl 4.8E3 46
^{28}S	^{29}S	^{30}S 5.7E4 42	^{31}S 3.5E7 45	^{32}S	^{33}S	^{34}S	^{35}S 1.1E8 35	^{36}S	^{37}S 6.1E7 48	^{38}S 1.7E7 48	^{39}S 1.6E5 47	^{40}S 4.1E2 49
^{27}P	^{28}P 5.8E4 42	^{29}P 1.3E6 43	^{30}P 1.1E7 43	^{31}P	^{32}P 9.2E7 44	^{33}P 6.7E7 48	^{34}P 3.9E7 44	^{35}P 1.5E7 48	^{36}P	^{37}P 8.2E5 50	^{38}P 7.9E3 48	^{39}P
^{26}Si	^{27}Si 9.7E5 43	^{28}Si	^{29}Si	^{30}S	^{31}Si 3.5E7 45	^{32}Si 1.3E7 48	^{33}Si 3.5E6 52	^{34}Si 1.0E6 52	^{35}Si 1.9E5 49	^{36}Si 2.5E4 49	^{37}Si	^{38}Si
^{25}Al 9.2E5 44	^{26}Al 5.4E6 44	^{27}Al	^{28}Al 2.0E7 45	^{29}Al 1.2E7 45	^{30}Al 4.4E6 45	^{31}Al 1.0E6 52	^{32}Al 2.1E5 45	^{33}Al 3.1E4 52	^{34}Al 4.3E3 52	^{35}Al 5.0E2 52	^{36}Al 4.9 51	^{37}Al

FIGURE 9
Top: simulation of RIBs achievable with FRAISE, using ^{20}Ne as the primary beam. Bottom: simulation of RIBs achievable with FRAISE, using ^{40}Ar as the primary beam. The figure is taken from [34].

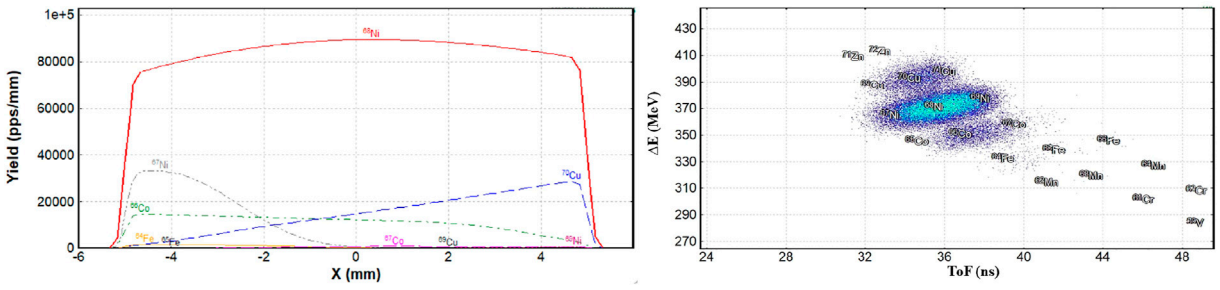

FIGURE 10
Left: simulated spatial distribution at the exit of the fragment separator on the horizontal direction and simulated ΔE-TOF (right), in the case of $^{70}Zn^{30+}$ primary beam at 40 AMeV and for a tuning of the fragment separator maximizing the ^{68}Ni production. For the sake of clarity, only the main contaminants are shown in the spatial distribution plot.

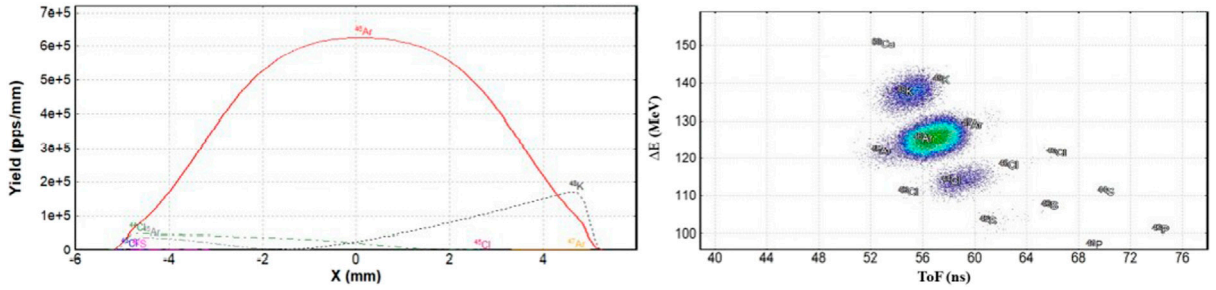

FIGURE 11
Left: simulated spatial distribution at the exit of the fragment separator on the horizontal direction and simulated ΔE-TOF tagging plot (right), in the case of $^{48}Ca^{20+}$ at 50 AMeV primary beam and for a tuning of the fragment separator maximizing the ^{46}Ar production. For the sake of clarity, only the main contaminants are shown in the spatial distribution plot.

did not obtain an advantage with respect to the use of ^{9}Be in any of the cases. At the energy available with the INFN-LNS CS, the focusing effect and the larger number of target atoms that can be used with ^{9}Be target compensate the higher pickup probability, guaranteed by a heavier target as ^{27}Al and ^{50}Ti, producing a smaller total yield. A better result could be obtained with smaller charge target, as lithium or deuterium targets, but at the present moment technological issues do not allow the easy use of such targets.

Some physics case opportunities with the use of FRAISE

FRAISE will be a very competitive facility for the production of light and medium mass unstable nuclei in the Fermi energy regime. Taking advantage of this apparatus, a plethora of studies concerning unstable nuclei close and far from the stability valley will be carried out. Among the different research topics, it could be possible to have the study of nuclei with neutron skin or nuclear halo structures. As an example, the investigation of the ^{8}B proton-halo structure could be performed using elastic and inelastic scattering on protons [31]. The ^{8}B isotope can be produced using a ^{12}C primary beam at 60 AMeV on a ^{9}Be target, with an intensity of 3.1×10^{6} pps and a purity of ≈50% (see Figure 7 left side). Another relevant case would be the study of the scattering of ^{11}Be on protons. ^{11}Be has received particular interest because of the inversion between $p_{1/2}$ and $s_{1/2}$ orbitals, and it presents a neutron-halo structure with resonances above the particle emission threshold [53]. In this case, a 1.5×10^{6} pps intensity is expected (see Figure 7 right side). Furthermore, using FRAISE, the investigation of nuclei with a neutron excess and their link with an excitation mode, known as pygmy dipole resonance (PDR), could be carried out. In detail, it could be important to investigate the PDR in the region of light and medium nuclei, such as ^{20}O, ^{34}Si, ^{38}S, ^{48}Ar, and ^{68}Ni. The aim is also to measure the neutron shell occupancy dependence of the PDR both below and above the particle emission threshold. Such topic would be investigated with high accuracy, thanks to the use of the CHIMERA multidetector and the FARCOS array in its complete configuration [54, 55]. The use of a new prototype of neutron detector could also be envisaged in order to fully characterize the PDR decay [56]. In addition, FRAISE will be able to deliver neutron-rich and neutron poor nuclei, such as $^{46,34}Ar$ and ^{68}Ni, allowing to extend the study of isospin effects in heavy-ion reactions at Fermi energies [57]. This topic has been widely explored with the CHIMERA multidetector [58–60]. The clustering structure of α particles in neutron-rich isotopes of Be, B, and C is another interesting topic that could be studied with FRAISE [61]. As an example, relevant cases are the clustering structures expected in ^{16}C and ^{10}Be. The ^{16}C and ^{10}Be structures were already investigated with the FRIBs facility [9, 61], but the collected statistics was just enough to extract the ^{16}C excitation energy spectrum and to speculate on new levels and still not enough for a quantitative assignment. With FRAISE, the yield of ^{16}C will increase to a factor of ≈20, and ^{10}Be will be produced with an intensity of 1.6×10^{7} pps [see Figure 7 (left side)], therefore, making this kind of measurement easily feasible. Another important case is the investigation of the ^{13}B clustering structure [62]. According to the antisymmetrized molecular dynamics (AMD) method calculations, the ^{13}B excited states exhibit cluster configurations with a large deformation leading to the appearance of rotational bands [63]. In the case of ^{13}B, FRAISE will deliver an intensity of 7.5×10^{6} pps [see Figure 7 (right side) and Figure 8]. Moreover, nuclear reactions of interest in the astrophysical context could be examined with FRAISE. Among the possible studies, we can mention the $^{14}O(\alpha, p)^{17}F$ reaction that could be the onset of a possible route that breaks out from the HCNO cycles, leading to the build-up of new elements [31] (in [31], further physics cases are discussed). Finally, also studies of interest for medical physics could be conducted. For instance, it is of particular interest the study of ^{11}C, whose β^{+}

decay would allow the simultaneous use of imaging techniques (using γ emitted by positron annihilation) and energy dissipation techniques [21, 22]. In this way, it could allow performing treatments and diagnostics at the same time, differing from the stable nuclei such as H, He, or C for hadron therapy techniques. Within this framework, the construction of the FRAISE facility offers a significant contribution in the panorama of nuclear physics.

Conclusion

In this paper, we reviewed the progress made at INFN-LNS for the production of high-quality and high-intensity RIBs, thanks to the use of the FRAISE facility. FRAISE is currently in its final construction phase, and next steps will deal with the test of the facility. In addition, essential steps for RIBs production are the tuning and transport processes, which require appropriate diagnostics and tagging devices. Such systems are under development, thanks to an R&D campaign started in these years. The diagnostics and tagging devices are based on SiC arrays coupled to fast custom frontend electronics; they allow the measurement of several features of RIBs and be able to operate in a highly radioactive environment, sustaining different experiments per year. The choice of the SiC technology has also been supported by RIBs simulations and preliminary tests. These feasibility studies also help in obtaining a reference study that identifies the opportunities offered by the FRAISE facility for the production of RIBs. The design of the SiC arrays and the development of the custom frontend are in their final phases, and the production phase of first test prototypes has been started. Further steps will concern the validation of prototypes and of the whole system, using radioactive sources, low-energy stable beams, and unstable nuclei. Furthermore, to reduce the beam commissioning time and enable a powerful control over the quality of the beam, we plan to develop innovative software tools based on machine learning.

Author contributions

All authors contributed to manuscript revision and read and approved the submitted version. NM: conceptualization, methodology, validation, formal analysis, investigation, writing—original draft, visualization, and supervision. GC: conceptualization, methodology, validation, investigation, visualization, supervision, and project administration. CG: conceptualization, methodology, validation, investigation, visualization, writing section of the paper. EP: conceptualization, methodology, validation, investigation, and visualization. AR: conceptualization, methodology, validation, investigation, and visualization. PR: conceptualization, methodology, validation, investigation, visualization, supervision, and project administration. LA: conceptualization, investigation, and visualization. AA: investigation and visualization. LCa: conceptualization, investigation, and visualization. AC, SC, LCo, MC, EF, GL, EG, BG, CM, SPa, SPi, GP, SPu, FRis, FRiz, DS, AT, MT, ST, and GV: investigation and visualization.

Funding

This research was partially supported by DGAPA-UNAM IN107820, the CONACYT 315839 projects and by the Italian Ministero dell'Istruzione, dell'Università e della Ricerca (MIUR) under PRIN contract 2020H8YFRE.

Acknowledgments

The authors would like to thank Andrea Naggi (Politecnico di Milano and INFN, Sezione di Milano) for his precious help in the design and qualification of the first prototypes of the SiC frontend electronics.

Conflict of interest

The authors declare that the research was conducted in the absence of any commercial or financial relationships that could be construed as a potential conflict of interest.

Publisher's note

Supplementary material

The Supplementary Material for this article can be found online at: https://www.frontiersin.org/articles/10.3389/fphy.2022.1058419/full#supplementary-material

References

1. Adamian GG, Antonenko NV, Diaz-Torres A, Heinz S. How to extend the chart of nuclides? *Eur Phys J A* (2020) 56:47. doi:10.1140/epja/s10050-020-00046-7

2. Ma CW, Wei HL, Liu XQ, Su J, Zheng H, Lin WP, et al. Nuclear fragments in projectile fragmentation reactions. *Prog Part Nucl Phys* (2021) 121:103911. doi:10.1016/j.ppnp.2021.103911

3. Mijatović T. Multinucleon transfer reactions: A mini-review of recent advances. *Front Phys* (2022) 10. doi:10.3389/fphy.2022.965198

4. Heinz S, Devaraja HM. Nucleosynthesis in multinucleon transfer reactions. *Eur Phys J A* (2022) 58:114. doi:10.1140/epja/s10050-022-00771-1

5. Nowacki F, Obertelli A, Poves A. The neutron-rich edge of the nuclear landscape: Experiment and theory. *Prog Part Nucl Phys* (2021) 120:103866. doi:10.1016/j.ppnp.2021.103866

6. Souliotis G, Stein B, Veselsky M, Galanopoulos S, Keksis A, Kohley Z, et al. Neutron-rich rare isotope production in the fermi energy domain and application to the Texas A&M radioactive beam upgrade. *Nucl Instr Methods Phys Res Section B: Beam Interactions with Materials and Atoms* (2008) 266:4692–6. doi:10.1016/j.nimb.2008.05.118

7. Freer M, Almaraz-Calderon S, Carter J, Aprahamian A, Ashwood NI, Barr M, et al. Simplicity from complexity. *J Phys : Conf Ser* (2012) 381:012009. doi:10.1088/1742-6596/381/1/012009

8. Freer M. The clustered nucleus-cluster structures in stable and unstable nuclei. *Rep Prog Phys* (2007) 70:2149–210. doi:10.1088/0034-4885/70/12/r03

9. Dell'Aquila D, Lombardo I, Acosta L, Andolina R, Auditore L, Cardella G, et al. New experimental investigation of the structure of ^{10}Be and ^{16}C by means of intermediate-energy sequential breakup. *Phys Rev C* (2016) 93:024611. doi:10.1103/PhysRevC.93.024611

10. Tanihata I, Hamagaki H, Hashimoto O, Shida Y, Yoshikawa N, Sugimoto K, et al. Measurements of interaction cross sections and nuclear radii in the light *p*-shell region. *Phys Rev Lett* (1985) 55:2676–9. doi:10.1103/PhysRevLett.55.2676

11. Tanihata I. Neutron halo nuclei. *J Phys G: Nucl Part Phys* (1996) 22:157–98. doi:10.1088/0954-3899/22/2/004

12. Bracco A, Lanza E, Tamii A. Isoscalar and isovector dipole excitations: Nuclear properties from low-lying states and from the isovector giant dipole resonance. *Prog Part Nucl Phys* (2019) 106:360–433. doi:10.1016/j.ppnp.2019.02.001

13. Minamisono T, Ohtsubo T, Minami I, Fukuda S, Kitagawa A, Fukuda M, et al. Proton halo of ^{8}B disclosed by its giant quadrupole moment. *Phys Rev Lett* (1992) 69:2058–61. doi:10.1103/PhysRevLett.69.2058

14. Spartà R, Di Pietro A, Figuera P, Tengblad O, Moro A, Martel I, et al. Probing proton halo effects in the ^{8}B+^{64}Zn collision around the coulomb barrier. *Phys Lett B* (2021) 820:136477. doi:10.1016/j.physletb.2021.136477

15. Aguilera EF, Amador-Valenzuela P, Martinez-Quiroz E, Lizcano D, Rosales P, Garcia-Martinez H, et al. Near-barrier fusion of the ^{88}**B** +^{58}Ni proton-halo system. *Phys Rev Lett* (2011) 107:092701. doi:10.1103/PhysRevLett.107.092701

16. Pakou A, Acosta L, O'Malley PD, Aguilar S, Aguilera EF, Baines M, et al. Dominance of direct reaction channels at deep sub-barrier energies for weakly bound nuclei on heavy targets: The case ^{8} B +^{208}Pb. *Phys Rev C* (2020) 102:031601. doi:10.1103/PhysRevC.102.031601

17. Mazzocco M, Keeley N, Boiano A, Boiano C, La Commara M, Manea C, et al. Elastic scattering for the ^{8}B and ^{7}Be +^{208}Pb systems at near-coulomb barrier energies. *Phys Rev C* (2019) 100:024602. doi:10.1103/PhysRevC.100.024602

18. Decrock P, Delbar T, Galster W, Huyse M, Leleux P, Licot I, et al. Radioactive beam investigation of the ^{13}N(p, γ)^{14}O reaction and the hot CNO cycle. *Phys Lett B* (1993) 304:50–4. doi:10.1016/0370-2693(93)91398-7

19. Belarge J, Kuvin S, Baby L, Baker J, Wiedenhover I, Hoflich P, et al. Experimental investigation of the ^{19}Ne(*p*, γ)^{20}Na reaction rate and implications for breakout from the hot CNO cycle. *Phys Rev Lett* (2016) 117:182701. doi:10.1103/PhysRevLett.117.182701

20. SPES project. *Spes: The hope of the legnaro national laboratory* (2022). Available at: https://web.infn.it/spes/ (Accessed September 30, 2022).

21. Boscolo D, Kostyleva D, Safari MJ, Anagnostatou V, Aysto J, Bagchi S, et al. Radioactive beams for image-guided particle therapy: The BARB experiment at GSI. *Front Oncol* (2021) 11:737050. doi:10.3389/fonc.2021.737050

22. Durante M, Parodi K. Radioactive beams in particle therapy: Past, present, and future. *Front Phys* (2020) 8:00326. doi:10.3389/fphy.2020.00326

23. Van Duppen P. Isotope separation on line and post acceleration. *The Euroschool Lectures Phys Exotic Beams* (2006) II:37–77.

24. Blumenfeld Y, Nilsson T, Van Duppen P. Facilities and methods for radioactive ion beam production. *Phys Scr* (2013) 152T:014023. doi:10.1088/0031-8949/2013/T152/014023

25. Anne R, Bazin D, Mueller A, Jacmart J, Langevin M. The achromatic spectrometer lise at ganil. *Nucl Instr Methods Phys Res Section A: Acc Spectrometers Detectors Associated Equipment* (1987) 257:215–32. doi:10.1016/0168-9002(87)90741-8

26. Geissel H, Armbruster P, Behr K, Brunle A, Burkard K, Chen M, et al. The GSI projectile fragment separator (FRS): A versatile magnetic system for relativistic heavy ions. *Nucl Instr Methods Phys Res Section B: Beam Interactions with Materials and Atoms* (1992) 70:286–97. doi:10.1016/0168-583x(92)95944-m

27. Wei J, Ao H, Beher S, Bultman N, Casagrande F, Chen J, et al. Advances of the FRIB project. In 14th International Conference on Heavy Ion Accelerator Technology (2019). MOYAA01. doi:10.18429/JACoW-HIAT2018-MOYAA01

28. Kubo T, Ishihara M, Inabe N, Kumagai H, Tanihata I, Yoshida K, et al. The RIKEN radioactive beam facility. *Nucl Instr Methods Phys Res Section B: Beam Interactions with Materials and Atoms* (1992) 70:309–19. doi:10.1016/0168-583x(92)95947-p

29. Tshoo K, Chae H, Park J, Moon J, Kwon Y, Souliotis G, et al. Design status of kobra for rare isotope production and direct measurements of radiative capture cross sections. *Nucl Instr Methods Phys Res Section B: Beam Interactions with Materials and Atoms* (2016) 376:188–93. doi:10.1016/j.nimb.2015.12.025

30. POTLNS project (2022). Available at: https://potlns.lns.infn.it/ (Accessed September 30, 2022).

31. Russotto P, Calabretta L, Cardella G, Cosentino G, De Filippo E, Gnoffo B, et al. Status and perspectives of the INFN – LNS in-flight fragment separator. *J Phys : Conf Ser* (2018) 1014:012016. doi:10.1088/1742-6596/1014/1/012016

32. Russo A, Calabretta L, Cardella G, Russotto P. Preliminary design of the new fragment in-flight separator (fraise). *Nucl Instr Methods Phys Res Section B: Beam Interactions with Materials and Atoms* (2020) 463:418–20. doi:10.1016/j.nimb.2019.04.037

33. Martorana NS. Status of the fraise facility and diagnostics system. *Il Nuovo Cimento 44 C* (2021) 1. doi:10.1393/ncc/i2021-21001-2

34. Martorana NS, Acosta L, Altana C, Amato A, Calabretta L, Carde G, et al. The new fragment in-flight separator at infn-lns. *Il Nuovo Cimento 45 C* (2022) 63. doi:10.1393/ncc/i2022-22063-2

35. Raciti G, Rapisarda E, De Napoli M, Amorini F, Calabretta L, Cardella G, et al. Intermediate energies tagged ribs. *Nucl Instr Methods Phys Res Section B: Beam Interactions Mater AtomsProceedings XVth Int Conf Electromagn Isotope Separators Tech Relat their Appl* (2008) 266:4632–6. doi:10.1016/j.nimb.2008.05.153

36. Raciti G, Rapisarda E, De Napoli M, Calabretta L, Cardella G, Giacoppo F, et al. Tagged intermediate energies radioactive ion beams at LNS. *Nucl Phys A* (2010) 834:780c–3c. doi:10.1016/j.nuclphysa.2010.01.145

37. Lombardo I, Amorini F, Cardella G, Cavallaro S, De Filippo E, Geraci E, et al. Use of large surface microchannel plates for the tagging of intermediate energy exotic beams. *Nucl Phys B - Proc Supplements* (2011) 215:272–4. doi:10.1016/j.nuclphysbps.2011.04.028

38. Martorana NS, Cardella G, Lanza E, Acosta L, Andres M, Auditore L, et al. First measurement of the isoscalar excitation above the neutron emission threshold of the pygmy dipole resonance in ^{68}Ni. *Phys Lett B* (2018) 782:112–6. doi:10.1016/j.physletb.2018.05.019

39. Raciti G, Cardella G, De Napoli M, Rapisarda E, Amorini F, Sfienti C. Experimental evidence of ^{2}He decay from ^{18}Ne excited states. *Phys Rev Lett* (2008) 100:192503. doi:10.1103/PhysRevLett.100.192503

40. Acosta L, Amorini F, Auditore L, Berceanu I, Cardella G, Chatterjiee M, et al. Kinematical coincidence method in transfer reactions. *Nucl Instr Methods Phys Res Section A: Acc Spectrometers Detectors Associated Equipment* (2013) 715:56–61. doi:10.1016/j.nima.2013.03.028

41. Grévy S, Hue R. Clim : The new rotating target for exotic nuclei production at LISE spectrometer. In: *24th world conference of the international nuclear target development society - intds2008*. Caen, France (2008).

42. Cappuzzello F, Agodi C, Carbone D, Cavallaro M. The MAGNEX spectrometer: Results and perspectives. *Eur Phys J A* (2016) 52:167. doi:10.1140/epja/i2016-16167-1

43. Tudisco S, La Via F, Agodi C, Altana C, Borghi G, Boscardin M, et al. Sicilia—Silicon carbide detectors for intense luminosity investigations and applications. *Sensors* (2018) 18:2289. doi:10.3390/s18072289

44. Risitano F. Simulation study of radioactive ion beams production at FRAISE(INFN – LNS). *Il Nuovo Cimento* (2022) 45:68. doi:10.1393/ncc/i2022-22068-9

45. Altana C, Cardella G, Castoldi A, Costa M, De Filippo E, Geraci E, et al. Feasibility study of a smart rad-hard fast detection system for radioactive ion beam tagging and diagnostics. In: *2021 IEEE nuclear science symposium and medical imaging conference (NSS/MIC)* (2021). p. 1–4. doi:10.1109/NSS/MIC44867.2021.9875842

46. Acosta L. NSS IEEE Conference records. *In preparation* (2022).

47. Castoldi A. Feasibility study of the use of operational amplifiers as forward gain stages in charge preamplifiers and shaping filters for radiation detectors. *Submitted IEEE Trans Nucl Sci* (2022).

48. Nania RC, Agodi F, Cappuzzello G, Cardella GAP, Cirrone E, De Filippo A, et al. Nuclear physics midterm plan at LNS. *in preparation* (2022).

49. Souliotis G, Koulouris S, Cappuzzello F, Carbone D, Pakou A, Agodi C, et al. Identification of medium mass (A=60–80) ejectiles from 15 MeV/nucleon peripheral heavy-ion collisions with the MAGNEX large-acceptance spectrometer. *Nucl Instr Methods Phys Res Section A: Acc Spectrometers, Detectors Associated Equipment* (2022) 1031:166588. doi:10.1016/j.nima.2022.166588

50. Fountas PN, Souliotis GA, Veselsky M, Bonasera A. Systematic study of neutron-rich rare isotope production in peripheral heavy-ion collisions below the fermi energy. *Phys Rev C* (2014) 90:064613. doi:10.1103/PhysRevC.90.064613

51. Papageorgiou A, Souliotis GA, Tshoo K, Jeong SC, Kang BH, Kwon YK, et al. Neutron-rich rare isotope production with stable and radioactive beams in the mass range A ≈ 40–60 at beam energy around 15 MeV/nucleon. *J Phys G: Nucl Part Phys* (2018) 45:095105. doi:10.1088/1361-6471/aad7df

52. Palli K, Souliotis GA, Depastas T, Dimitropoulos I, Fasoula O, Koulouris S, et al. Microscopic dynamical description of multinucleon transfer in ^{40}Ar induced peripheral collisions at 15 MeV/nucleon. *EPJ Web Conf* (2021) 252:07002. doi:10.1051/epjconf/202125207002

53. Talmi I, Unna I. Order of levels in the shell model and spin of ^{11}Be. *Phys Rev Lett* (1960) 4:469–70. doi:10.1103/PhysRevLett.4.469

54. Badalà A, La Cognata M, Nania R, Osipenko M, Piantelli S, Turrisi R, et al. Trends in particle and nuclei identification techniques in nuclear physics experiments. *Riv Nuovo Cim* (2022) 45:189–276. doi:10.1007/s40766-021-00028-5

55. Geraci E, Acosta L, Cardella G, Castoldi A, De Filippo E, Gnoffo B, et al. Highlights from chimera collaboration. *Il Nuovo Cimento 45 C* (2022) 44. doi:10.1393/ncc/i2022-22044-5

56. Pagano EV, Acosta L, Cardella G, De Filippo E, Geraci E, Gnoffo E, et al. Recent results on the construction of a new correlator for neutrons and charged particles and for farcos. *Il Nuovo Cimento 45 C* (2022) 64. doi:10.1393/ncc/i2022-22064-1

57. Borderie B, Rivet M, Tassan-Got L. Heavy-ion peripheral collisions in the fermi energy domain : Fragmentation processes or dissipative collisions. *Ann Phys (Paris)* (1990) 15:287–390. doi:10.1051/anphys:01990001504028700

58. Cardella G, Giuliani G, Lombardo I, Papa M, Acosta L, Agodi C, et al. Effects of neutron richness on the behavior of nuclear systems at intermediate energies. *Phys Rev C* (2012) 85:064609. doi:10.1103/PhysRevC.85.064609

59. Russotto P, De Filippo E, Pagano A, Acosta L, Auditore L, Baran V, et al. Production cross sections for intermediate mass fragments from dynamical and statistical decay of projectile-like fragments in ^{124}Sn +^{64}Ni and ^{112}Sn +^{58}Ni collisions at 35 AMeV. *Phys Rev C* (2015) 91:014610. doi:10.1103/PhysRevC.91.014610

60. Russotto P, De Filippo E, Pagano EV, Geraci E, Maiolino C, Martorana NS, et al. Status of data analysis and preliminary results of the CHIFAR experiment. *IL NUOVO CIMENTO 45 C* (2022) 55. doi:10.1393/ncc/i2022-22055-2

61. Risitano F, Acosta L, Cardella G, De Filippo E, Dell'Aquila D, Favela F, et al. Status of the CLIR experiment at LNS. *IL NUOVO CIMENTO 45C* (2022) 60. doi:10.1393/ncc/i2022-22060-5

62. Gnoffo B, Pirrone S, Politi G, Cardella G, De Filippo E, Geraci E, et al. Clustering and molecular states in neutron rich nuclei. *Contrib this volume* (2022).

63. Di Pietro A, Fernandez-Garcia JP, Ferrera F, Figuera P, Fisichella M, Lattuada M, et al. Experimental investigation of exotic clustering in ^{13}B and ^{14}C using the resonance scattering method. *J Phys : Conf Ser* (2018) 966:012040. doi:10.1088/1742-6596/966/1/012040